ACS Catalysis

Research Article

pubs.acs.org/acscatalysis

Thermodynamic and Structural Factors That Influence the Redox Potentials of Tungsten−Alkylidyne Complexes

Benjamin Rudshteyn,[†] Hunter B. Vibbert,[‡] Richard May,[†] Eric Wasserman,[†] Ingolf Warnke,[†] Michael D. Hopkins,*[,‡] and Victor S. Batista*[,†]

[†]Department of Chemistry and Energy Sciences Institute, Yale University, New Haven, Connecticut 06520, United States

[‡]Department of Chemistry, University of Chicago, Chicago, Illinois 60637, United States

Supporting Information

ABSTRACT: The thermodynamic and structural factors that influence the redox properties of an extensive set of tungsten−alkylidyne complexes ($W(CR)L_4X$) are analyzed by combining synthesis, electrochemistry, and computational modeling based on free energy calculations of oxidation potentials at the density functional theory level. The observed linear correlations among oxidation potentials, HOMO energies, and gas-phase ionization energies are found to be consistent with the approximately constant solvation free energy differences between reduced and oxidized species over the complete set. The W−X bond length, *trans* to the alkylidyne ligand, is found to be a good descriptor of the positioning of the key frontier orbitals that regulate the redox properties of the complexes.

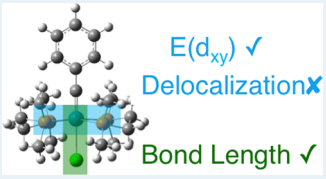

KEYWORDS: *redox potentials, tungsten−alkylidyne complex, density functional theory, photoredox chromophores, descriptor*

INTRODUCTION

Understanding the electronic and structural factors that govern the redox properties of transition metal complexes is centrally important to much of inorganic chemistry. Computational approaches that accurately reproduce experimental redox potentials offer the possibility of both understanding these potentials in terms of underlying thermodynamic quantities and designing new complexes with specific properties.[1,2] One of many areas where computational design could play an important role is in the development of new photoredox chromophores with applications in solar fuels and organic synthesis.[3−6] The excited-state redox potential of a photoredox chromophore is governed by the ground-state redox potential and the excited-state energy; these quantities are independently computable, whereas empirical prediction of their sum can be difficult for new compounds because variations within the coordination sphere affect the energies in ways that are not straightforwardly separable.

One family of photoredox chromophores with desirable properties is comprised of tungsten−alkylidyne complexes of the form $W(CR)L_4X$ (L is a neutral ligand, and X is an anionic ligand).[7,8] These luminescent d^2 complexes have oxidation potentials that can be tuned over the unusually broad range of 2 V,[9] which suggests a corresponding level of control can be exercised over their excited-state redox potentials. In addition, the structures of these complexes are characterized by small distortions among their ground, excited, and oxidized (d^1) states, evincing correspondingly small inner-sphere reorganization energies for their redox reactions.[10] Finally, the chromophore can be regenerated following oxidation via reaction with H_2, providing a means of closing a solar-fuel cycle with renewable reducing equivalents rather than conventional sacrificial donors.[11] We reported an electrochemical study of the effects on the oxidation potentials of $W(CR)L_4X$ compounds resulting from variation of the CR, L, and X ligands across 32 derivatives [**1**−**32** (Chart 1)].[9] It was observed that the oxidation potential is significantly more sensitive to the nature of the L ligands than to the CR and X ligands, consistent with the fact that the d_{xy} redox orbital has π symmetry with respect to the equatorial L ligands and is nonbonding (δ symmetry) with respect to the axial X and CR ligands. It was also found that there is a strong linear correlation (with a slope of $\cong$1) between the experimentally measured oxidation potential and the calculated energy [density functional theory (DFT)] of the redox orbital. There were notable outliers in this correlation, however, and it was further observed, surprisingly, that the potential is not correlated with the calculated relative d_{xy}/L atomic parentage of the redox orbital. The application of more sophisticated computational methods for redox properties offers the possibility of understanding the positive and negative correlations among this broad range of complexes in terms of underlying structural and thermodynamic factors.

Here, we use the Born−Haber cycle[1] theoretical framework that partitions calculated free energy contributions into the gas-phase free energy and solvation energies of the d^2 (reactant) and d^1 (product) species of $W(CR)L_4X$ oxidation reactions (Scheme 1). Values obtained from the free energy calculations can be directly correlated to experimental oxidation potentials through use of an oxidation potential standard. This methodology has been applied to the original set of 32 complexes and

Received: May 19, 2017
Revised: July 7, 2017
Published: July 14, 2017

DOI: 10.1021/acscatal.7b01636
ACS Catal. 2017, 7, 6134−6143

Chart 1. Tungsten−Alkylidyne Complexes Investigated in This Study[a]

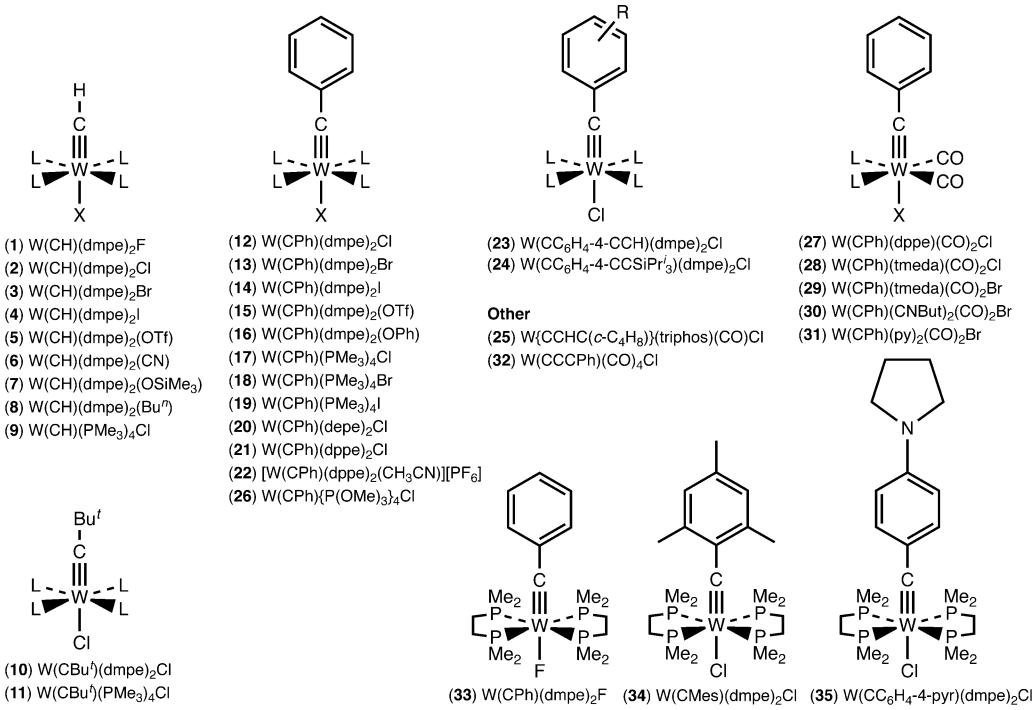

[a]Abbreviations: dmpe, $Me_2PCH_2CH_2PMe_2$; depe, $Et_2PCH_2CH_2PEt_2$; dppe, $Ph_2PCH_2CH_2PPh_2$; tmeda, 1,2-$Me_2NCH_2CH_2NMe_2$; triphos, $PPh(CH_2CH_2PPh_2)_2$.

Scheme 1. Born−Haber Method for Calculating Oxidation Potentials with a Generic Tungsten−Alkylidyne Complex, W(CR)L$_4$X[a]

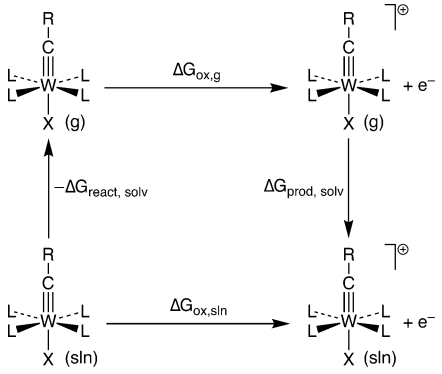

$$\Delta G_{ox,sln} = -\Delta G_{react,\ solv} + \Delta G_{ox,g} + \Delta G_{prod,\ solv}$$

[a]The reactant is the neutral d^2-configured species, and the product is the d^1-configured oxidized species. "Solv" refers to solvation, "sln" to solution, and "ox" to oxidation.

three new derivatives [**33**−**35** (Chart 1)] that broaden the variation of the CR and X groups. In general, we find good agreement between theory and experiment. Further analysis of the partitioned free energy contributions shows that the net solvation energy spans a narrow range for these compounds, consistent with the previously observed linear correlation between oxidation potential and redox orbital energy. Spin density calculations on the d^1 (product) complexes demonstrate that the SOMO is of metal-centered d_{xy} parentage. However, we observe only a very coarse overall correlation between the spin density on tungsten and the energy of the d_{xy} redox orbital. Finally, we find that the W−X bond length is a reporter of the oxidation potential: complexes with longer W−X bonds are easier to oxidize, with the bond length and potential being linearly related. This relatively simple, low-level DFT method provides a convenient, accurate computational model that can be used to predict the oxidation potentials for new or previously unstudied tungsten−alkylidyne chromophores.

METHODS

Experimental Methods. The new complexes W(CPh)(dmpe)$_2$F (**33**) and W(CC_6H_4-4-pyr)(dmpe)$_2$Cl (**35**; pyr = *N*-pyrrolidyl) were synthesized using routes and procedures similar to those employed for related complexes and were characterized by multinuclear nuclear magnetic resonance (NMR) spectroscopy, mass spectrometry, elemental analyses, and X-ray crystallography; full details of their preparation and characterization are provided in the Supporting Information. The compound W(CMes)(dmpe)$_2$Cl (**34**; Mes = 2,4,6-$C_6H_2Me_3$) was prepared according to the standard procedure.[12]

Electrochemical measurements [cyclic voltammetry (CV) and differential pulse voltammetry (DPV)] were performed at room temperature in a nitrogen-filled glovebox using a Bioanalytical Systems 100 B/W Electrochemical Workstation. A three-electrode configuration was used, which consisted of a working electrode (platinum disk), an auxiliary electrode (platinum disk), and a quasi-reference electrode (silver wire). Samples ranged in concentration from 0.3 to 2.0 mM analyte in a tetrahydrofuran (THF) solution with 0.1 M [Bu^n_4N][PF_6]. The electrochemical reversibility of redox couples was established via Randles−Sevcik plots of CV data. Electrode potentials are referenced to $FeCp_2^{0/+}$. Full experimental details and data pertaining to the electrochemical measurements are provided in the Supporting Information.

DOI: 10.1021/acscatal.7b01636
ACS Catal. 2017, 7, 6134−6143

Single-crystal X-ray diffraction measurements of **12**, **33**, and **35** were performed using a Bruker D8 VENTURE with PHOTON 100 CMOS detector system equipped with a Mo target X-ray tube (λ = 0.71073 Å). Full details regarding data acquisition and structure refinement are provided in the Supporting Information.

Computational Modeling Methods. DFT calculations were performed using the B3LYP[13] exchange-correlation functional as implemented in the Gaussian 09 software package.[14] The basis set consisted of LANL2DZ[15] for W, Cl, Br, and I, while the 6-311G* basis was used for all other atoms; a structural benchmarking study of **12**, **21**, **21**$^+$, **33**, and **35** indicated that this level of theory provided good agreement with experiment (Tables S8 and S9). Solvation free energies were calculated using the SMD dielectric continuum model[16] for the specific solvents used for measurements on a given compound (ε = 7.43 for THF, ε = 35.7 for acetonitrile, and ε = 8.93 for dichloromethane). The overall methodology and modest level of theory are comparable to methods implemented successfully in previous studies of redox couple systems.[1]

Symmetry constraints were allowed, with convergence criteria for optimization ("tight" keyword) in atomic units of 1.0×10^{-5} for the root-mean-square (RMS) force threshold, 1.5×10^{-5} for the maximal force threshold, 4.0×10^{-5} for the RMS displacement threshold, and 6.0×10^{-5} for the maximal displacement threshold.[14] The integration grid consisted of 99 radial shells with 590 angular points each ("ultrafine" keyword).[14]

All complexes were modeled as d^2 W(IV) spin singlets[14] in their reduced form and d^1 W(V) spin doublets in their oxidized form. Triplets were not considered as the lowest triplet ground state is generally ~2 eV above the ground state in these systems.[8] The redox potential ($E_{1/2}$) for each pair of d^2/d^1 (reactant/product) complexes was computed, using the Born–Haber cycle (Scheme 1),[1] relative to the computed potential of W(CPh)(dmpe)$_2$Cl (**12**). Complex **12** was chosen as the reference compound because it has an electrochemically reversible d^2/d^1 couple and has CPh, dmpe, and Cl ligands commonly found among the 35 derivatives in this study. The computed $E_{1/2}$ for **12** was corrected to fit the experimental value of −0.82 V.[9] Equation 1 gives the expression for $E_{1/2}$.

$$E_{1/2} = \frac{\Delta G_{ox,sln}}{nF} = \frac{-\Delta G_{reac,solv} + \Delta G_{ox,g} + \Delta G_{prod,solv}}{nF} \quad (1)$$

where F is the Faraday constant, n is the number of moles of electrons involved in the redox reaction (here, n = 1), and $\Delta G_{reac,solv}$, $\Delta G_{ox,g}$, and $\Delta G_{prod,solv}$ correspond to the free energy of solvation for the reactant, the gas-phase oxidation free energy change, and the free energy of solvation of the product, respectively. All free energies include room-temperature thermal corrections, as implemented in Gaussian 09.[17] The gas-phase optimized geometries were used to obtain gas-phase free energy changes $\Delta G_{ox,g}$ as well as solvation free energies $\Delta G_{reac,solv}$ and $\Delta G_{prod,solv}$, including the effect of the dielectric continuum on the vibrations and thus the entropy terms.[18,19] This approach would be close to a direct calculation of free energies (including vibrational corrections) in the dielectric continuum except for the approximation that the solvent does not significantly change the geometry of the solute. Direct calculations perform as well as true thermodynamic cycles or better when the solvated structure and/or vibrations vary heavily compared to the gas-phase structure,[2,20] but the Born–Haber approach can more effectively cancel out error when the geometry of the reactant responds to solvation in a manner similar to that of the product, which applies in the case of tungsten–alkylidyne complexes that mostly undergo small changes in their W–X bond length when solvated. The Born–Haber cycle allows for the isolation of which free energy term is causing most of the error and was found to perform better than using the parametrized single-point energies for the solvation steps. We additionally considered a select number of molecules to optimize in the dielectric continuum and found that the errors are either similar or worse than using the gas-phase geometries (Table S12).

RESULTS AND DISCUSSION

Electrochemical Properties of W(CR)L$_4$X Complexes. To investigate the effects on oxidation potentials of R and X

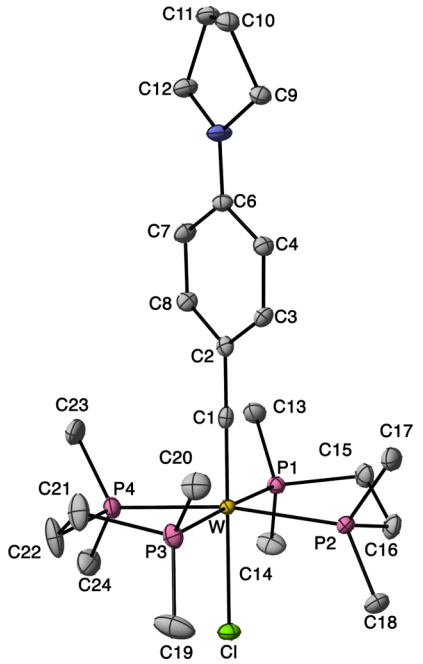

Figure 1. Thermal ellipsoid representation of the molecular structure of **35** (50% probability ellipsoids). Hydrogen atoms, interstitial THF, and the disorder within one of the dmpe ligands are not shown.

Table 1. Oxidation Potentials for Selected W(CR)L$_4$X and W(CR)L$_2$L′$_2$X Complexes[a]

compound	$E_{1/2}$ (V vs $FeCp_2^{0/+}$)
W(CPh){P(OMe)$_3$}$_4$Cl (**26**)	−0.24[b,c]
W(CPh)(dppe)(CO)$_2$Cl (**27**)	0.68[b,d]
W(CPh)(tmeda)(CO)$_2$Cl (**28**)	0.39[b,e]
W(CPh)(dmpe)$_2$F (**33**)	−0.91[f]
W(CMes)(dmpe)$_2$Cl (**34**)	−0.87[f]
W(CC$_6$H$_4$-4-pyr)(dmpe)$_2$Cl (**35**)	−0.93[f]

[a]THF solution with 0.1 M [Bu$^n_4$N][PF$_6$]. [b]Measured by DPV. [c]Reported in ref 9 by CV as quasi-reversible at room temperature and as −0.28 V at −13 °C. [d]Reported in ref 9 by CV as E_p = 0.66 V (irreversible). [e]Reported in ref 9 by CV as E_p = 0.41 V (irreversible). [f]Measured using CV. The potential measured by DPV is within 0.01 V of this value.

DOI: 10.1021/acscatal.7b01636
ACS Catal. 2017, 7, 6134–6143

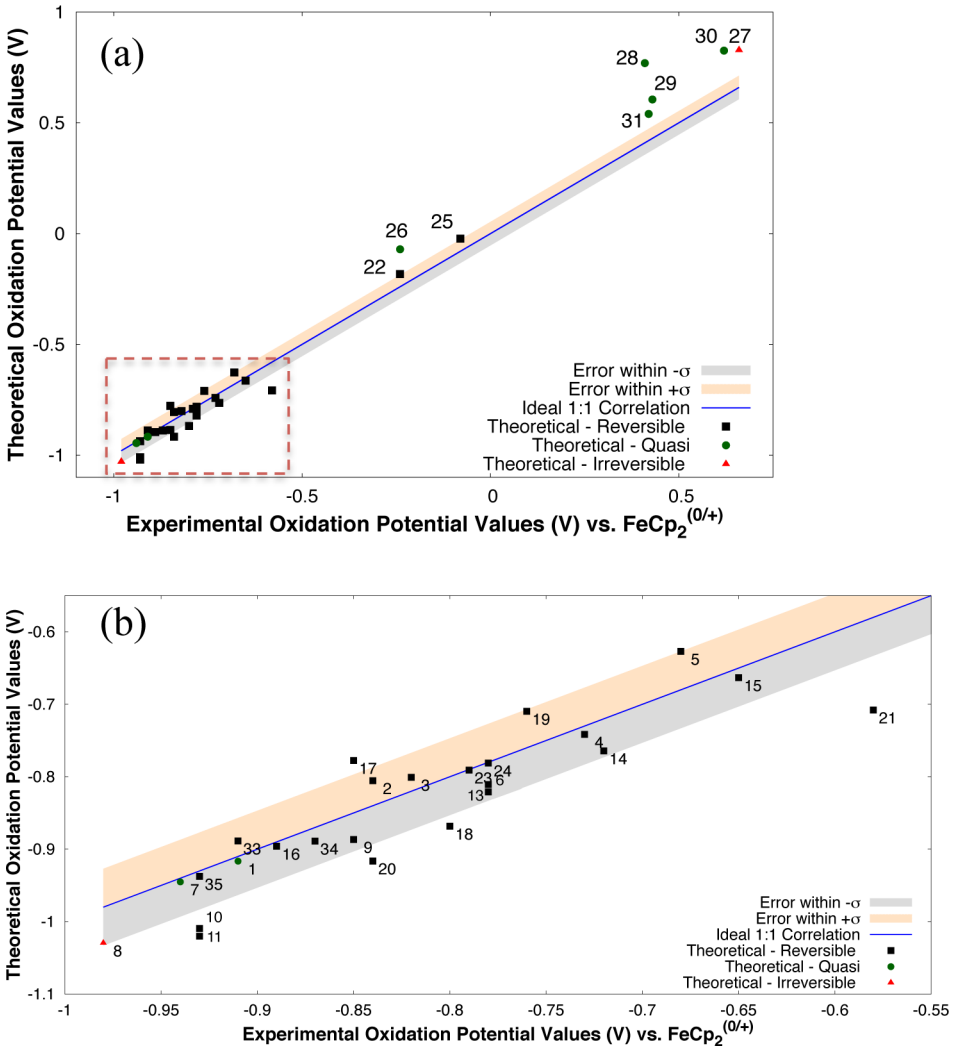

Figure 2. Relationship between calculated and experimental oxidation potentials: (a) all compounds except **12** (the reference compound) and **32** (for which an experimental value is not available) and (b) expansion of the region in panel a within the red dashed-line box, containing compounds of the form W(CR)L_4X (L = phosphine). The blue line corresponds to an ideal 1:1 correlation between theory and experiment. The colored bands indicate a $\pm\sigma$ region relative to the experimental axis (see the text for error analysis). Points are labeled with the complex number.

substituents not encompassed by the original set of 32 W(CR)L_4X compounds [**1**−**32** (Chart 1)],[9] the oxidation potentials of three additional tungsten−alkylidyne complexes were measured [**33**−**35** (Chart 1)]. The effects of incorporating electron-donating groups on the commonly employed benzylidyne CR ligand were probed via a study of the methyl- and amine-substituted derivatives W(CMes)(dmpe)$_2$Cl (**34**; Mes = 2,4,6-$C_6H_2Me_3$)[12] and W(CC_6H_4-4-pyr)(dmpe)$_2$Cl (**35**; pyr = *N*-pyrrolidyl). In addition, the effect of a fluoro X ligand was assessed via a study of complex W(CPh)(dmpe)$_2$F (**33**); the only fluoro derivative in the original set [W(CH)(dmpe)$_2$F (**1**)] exhibited a quasi-reversible oxidation, which was unusual because chloro, bromo, and iodo derivatives generally exhibit reversible oxidations.[9] The reference compound for evaluating the effects of these substituents is W(CPh)(dmpe)$_2$Cl (**12**). To determine whether these substituents significantly perturb the molecular structures of the compounds, which would complicate comparisons of their redox properties, the structures of **12** (Figure S14), **33** (Figure S15), and **35** (Figure 1) were determined by single-crystal X-ray diffraction studies. The core bond distances and angles of the three compounds are essentially identical, with the W≡C and W−P bond lengths differing from each other by less than 3σ (Table S7). Of note for pyrrolidyl derivative **35** (Figure 1) are the facts that this substituent exhibits a planar geometry at the nitrogen atom [sum of C−N−C angles of 359° (Table S6)] and is approximately coplanar with the phenyl ring (dihedral angle of ≅6°), consistent with maximal electron donation by the pyrrolidyl group.

The oxidation potentials of W(CPh)(dmpe)$_2$F (**33**), W(CMes)(dmpe)$_2$Cl (**34**; Mes = 2,4,6-$C_6H_2Me_3$), and W(CC_6H_4-4-pyr)(dmpe)$_2$Cl (**35**) were determined by cyclic (CV) and differential pulse (DPV) voltammetry (Table 1 and Figures S20−S22). The compounds display a reversible $W^{IV/V}$ couple. The oxidation potentials of **34** ($E_{1/2}$ = −0.87 V) and **35** ($E_{1/2}$ = −0.93 V) are lower than those of parent benzylidyne complex W(CPh)(dmpe)$_2$Cl (**12**; $E_{1/2}$ = −0.82 V)[9] and lie in the order consistent with the electron-donating ability of the phenyl substituent (R: Ph > Mes > C_6H_4-4-pyr). These results demonstrate the possibility of fine-tuning the redox potential via benzylidyne substituents despite the orthogonality of alkylidyne−ligand orbitals to the d_{xy} redox orbital. The reversible oxidation exhibited by fluoro derivative W(CPh)(dmpe)$_2$F (**33**; $E_{1/2}$ = −0.91 V) contrasts with the quasi-

DOI: 10.1021/acscatal.7b01636
ACS Catal. 2017, 7, 6134−6143

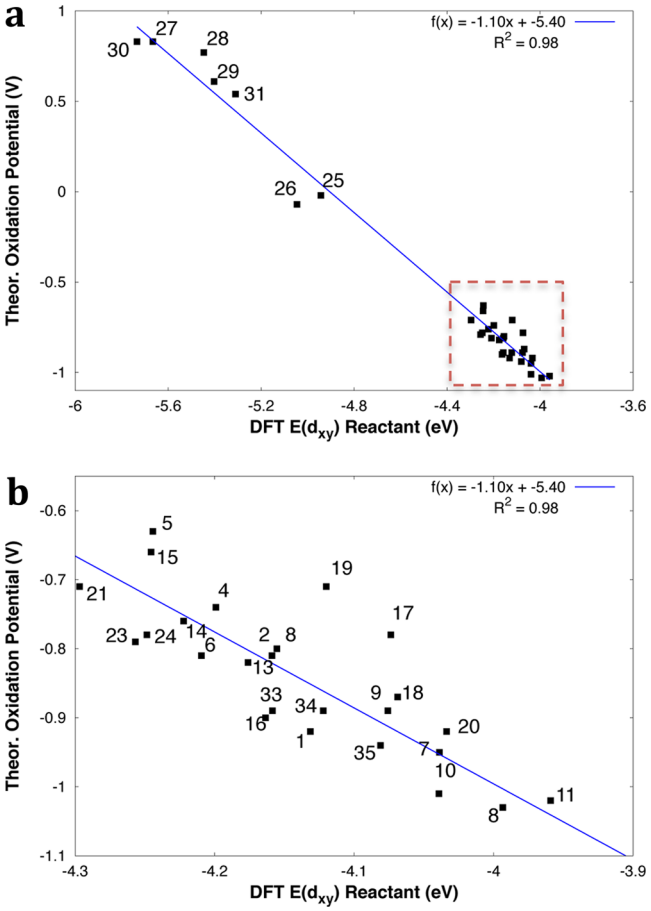

Figure 3. (a) Correlation between theoretical oxidation potentials and the DFT energy of the frontier orbital with d_{xy} character for all complexes except **12**, **22**, and **32**, with an expansion (b) of the region between −4.3 and −3.9 eV (area within the red dashed-line box, top).

reversible process noted above for W(CH)(dmpe)$_2$F (**1**)[9] but is in line with the reversibility observed for all other halide derivatives with phosphine ligands (X = Cl, Br, or I; **2**−**4**, **9**−**14**, **17**−**21**, **23**, and **24**). The negative shift of the oxidation potential of **33** relative to that of the chloro analogue **12** ($\Delta E_{1/2}$ = 0.09 V) is close to the difference between W(CH)(dmpe)$_2$F (**1**) and W(CH)(dmpe)$_2$Cl (**2**) ($\Delta E_{1/2}$ = 0.07 V).[9]

Within the original set of 32 compounds, complex W(CPh){P(OMe)$_3$}$_4$Cl (**26**) and all those of the form W(CPh)L$_2$(CO)$_2$X (L = $^1/_2$dppe, X = Cl, **27**; L = $^1/_2$tmeda, X = Cl, **28**; L = $^1/_2$tmeda, X = Br, **29**; L = CNBu^t, X = Br, **30**; L = py, X = Br, **31**) were observed to exhibit quasi-reversible or irreversible oxidations in CV experiments at room temperature.[9] To determine whether the reported CV peak potentials are close enough to the actual oxidation potentials to be suitable for comparison to theoretically computed values, the oxidation potentials ($E_{1/2}$) of **26**−**28** were measured by DPV[21] (Table 1 and Figures S18 and S19). The difference between the DPV potentials and CV peak potentials is only 0.02−0.04 V, suggesting that the CV peak potentials are good approximations of the oxidation potentials for this set of compounds.

Correlation between Calculated and Experimental Oxidation Potentials. The relationship between the experimentally measured and computed oxidation potentials of W(CR)L$_4$X complexes **1**−**35** is shown in Figure 2, and the calculated thermodynamic quantities that contribute to $E_{1/2}$ ($\Delta G_{reac,solv}$, $\Delta G_{ox,g}$, and $\Delta G_{prod,solv}$) are set out in Table S10. The complexes fall into two broad classes with regard to the agreement between theoretical and experimental values. W(CR)L$_4$X compounds that have exclusively phosphine equatorial ligands (**1**−**21** and **33**−**35**), which exhibit reversible oxidations with $E_{1/2}$ values of less than −0.5 V, show good agreement between the theoretical and experimental oxidation potentials: most lie near the line of perfect agreement (slope = 1, intercept = 0). Compounds of the form W(CR)L$_2$(CO)$_2$X (**27**−**31**), which exhibit quasi-reversible or irreversible oxidations with $E_{1/2}$ values of >0.3 V, clearly lie above the line of ideal agreement. Three compounds with singular compositions lie between these two clusters of complexes: [W(CPh)(dppe)$_2$(NCMe)]$^+$ (**22**), which is the only cationic compound in the set; phosphite derivative W(CPh){P(OMe)$_3$}$_4$Cl (**26**), which exhibits a quasi-reversible oxidation at room temperature and, similar to **27**−**31**, lies above the line; and W{CCHC(c-C$_4$H$_8$)}(triphos)(CO)Cl (**25**),[22] which is the sole monocarbonyl derivative.

A statistical evaluation of the agreement between theory and experiment was performed using the subset of 21 complexes that have fully reversible oxidations in THF solution at room temperature. The experimental and computed potentials for this set of compounds (**2**−**6**, **9**−**11**, **13**−**15**, **17**−**21**, **23**, **24**, and **33**−**35**) can be fit to a linear relationship (r^2 = 0.76) with a slope of 0.97 and an intercept of −0.04, which is close to the case of ideal agreement with a slope of 1 and an intercept of 0 (Figure S23). The agreement between theory and experiment was evaluated by examination of the distribution of values of $\Delta E = E_{theory} - E_{exp}$ (Figure S24); this provides the mean deviation μ = −4 mV [$\mu = (\sum \Delta E_n)/n$] and standard deviation σ = 46 mV. The distribution of binned mean deviation values was observed to be approximately Gaussian (Figure S24); the parameters obtained from a Gaussian fit [μ = −8 mV, and σ = 50 mV (Figure S24)] are in close agreement with the values given above, confirming that μ and σ are appropriate statistical parameters for evaluating the concordance of theoretical and experimental potentials. Over the 0.35 V range of measured oxidation potentials for this subset of compounds, the line of ideal agreement lies within the 1σ limits. The mean and standard deviations compare well with those derived in the earlier study[1] (μ = −2 mV, and σ = 64 mV), which employed a similar level of theory using a redox couple in the same row of the periodic table.

Although for the majority of compounds the computed and experimental oxidation potentials differ by less than one standard deviation, there are several others for which this is not the case. Among the subset of 21 complexes noted above used to determine the statistical metrics, the calculated oxidation potentials of complexes W(CBu^t)(dmpe)$_2$Cl (**10**), W(CBu^t)(PMe$_3$)$_4$Cl (**11**), W(CPh)(PMe$_3$)$_4$Cl (**17**), W(CPh)(PMe$_3$)$_4$Br (**18**), and W(CPh)(depe)$_2$Cl (**20**) differ from experiment by $|E_{theory} - E_{exp}|$ = 60−80 mV. These outliers do not share obvious common chemical features apart from the fact that they have multiple methyl groups on the L and/or R substituents. It is possible that these compounds have multiple structural minima with similar energies; a more accurate calculation of their oxidation potentials may require a Monte Carlo average over thermally accessible configurations. The largest deviations (>2σ) between theoretical and experimental potentials are found for W(CPh)(dppe)$_2$Cl (**21**), W(CPh){P(OMe)$_3$}$_4$Cl (**26**), and compounds of the form W(CPh)L$_2$(CO)$_2$X (**27**−**31**). As discussed below, these compounds share the same d_{xy} redox orbital as those compounds for which

DOI: 10.1021/acscatal.7b01636
ACS Catal. 2017, 7, 6134−6143

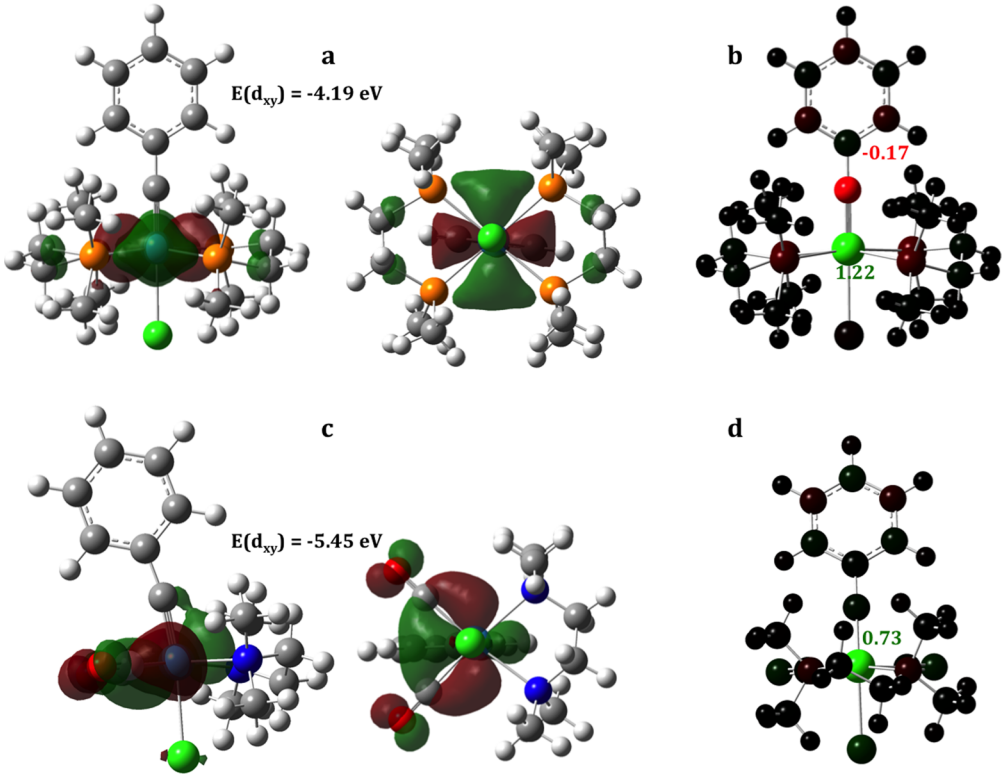

Figure 4. (a) Isosurface of the frontier orbital with d_{xy} character for **12** (isovalue = 0.04). (b) Mulliken spin population for $\mathbf{12}^+$ (the oxidized form of **12**), where red indicates β spin density (<−0.10), green indicates a very large α spin density (>0.5), maroon indicates slight β spin density (~0.03), and black indicates a negligible spin density. Panels c and d show analogous results for **28** and $\mathbf{28}^+$, respectively. Color key for isosurfaces in panels a and c: green and brown isosurfaces indicate positive and negative phases, respectively, of the frontier orbital. In panels a and c, atoms are represented as follows: white for H, blue for N, turquoise for W, orange for P, gray for C, and green for Cl.

the experimental and computed potentials are in close agreement. All but **21** exhibit quasi-reversible or irreversible oxidations; whether this is related to the deviation between theory and experiment is unclear. Except for compound **28**, which shows the largest deviation between theory and experiment, the DFT methodology nevertheless correctly predicts the trend in oxidation potential for these compounds. To probe whether higher levels of theory would improve the agreement with experiment, a calculation that accounts for dispersion utilizing Grimme's D3 empirical dispersion factor with Becke−Johnson damping (GD3BJ)[23] was performed on **21**, which is the one outlier in this group that exhibits an electrochemically reversible oxidation. This calculation decreased the difference between theory and experiment to 50 mV (1σ).

The fact that DFT methodology allows accurate (**1**−**20**, **22**−**25**, and **33**−**35**) and semiquantitative (**21** and **26**−**31**) prediction of the oxidation potential allows analysis of the trends in redox properties over the series of complexes by examination of the partitioned thermodynamic quantities $\Delta G_{\text{reac,solv}}$, $\Delta G_{\text{ox,g}}$, and $\Delta G_{\text{prod,solv}}$ (Scheme 1 and Table S10).[24] In our prior report, it was noted that the measured oxidation potentials of these compounds are correlated linearly with the calculated energy of the d_{xy} orbital of the d^2-configured reactant.[9] This result is reproduced by the calculations employed in the study presented here (Figure 3 and Figure S25). In addition, calculation of the symmetry of the total spin densities of the frontier orbitals for the oxidized (d^1) products (Table S11) confirms that the frontier orbital with d_{xy} character is the redox orbital for all complexes except W(CCCPh)-$(CO)_4$Cl (**32**), for which the d_{xy} orbital is HOMO−2. As one might expect, a corresponding relationship is also found between the experimental oxidation potential and the calculated ionization energy ($\Delta G_{\text{ox,g}}$) (Figure S26). As was suggested for the case of the correlation with the d_{xy} orbital energy, this result indicates that the solvation energy differences associated with oxidation are roughly constant across the series. Indeed, analysis of the solvation energies for the 32 complexes with experimental electrochemical data in THF (Figure S27) shows that $\Delta G_{\text{prod,solv}} - \Delta G_{\text{reac,solv}}$ varies only from −23 to −35 kcal/mol, indicating that the factors that control the energies of the frontier orbitals, summarized in Figure S28, are most responsible for the observed trends in oxidation potentials. The complexes that show the largest differences between computed and experimental oxidation potential (**21** and **26**−**31**, >2σ) also tend to be outliers in the correlation between $E_{1/2}$ and $\Delta G_{\text{ox,g}}$ (Figure S26) and have solvation energies that are clustered toward the edges of the overall range (Figure S27) but do not exhibit a systematic positive or negative skew in these quantities.

Electronic and Structural Factors Relevant to Oxidation Potentials. It was noted in the earlier report that the oxidation potentials of W(CR)L_4X compounds vary more strongly with substitution of the equatorial L ligands than with that of the CR and X ligands.[9] This observation was rationalized by noting that the d_{xy} redox orbital is nonbonding (δ symmetry) relative to the CR and X ligands and π symmetry with respect to the L ligands, thus allowing stronger electronic interactions between the d_{xy} orbital and the L ligands. Consistent with this expectation, comparison of the redox

DOI: 10.1021/acscatal.7b01636
ACS Catal. 2017, 7, 6134−6143

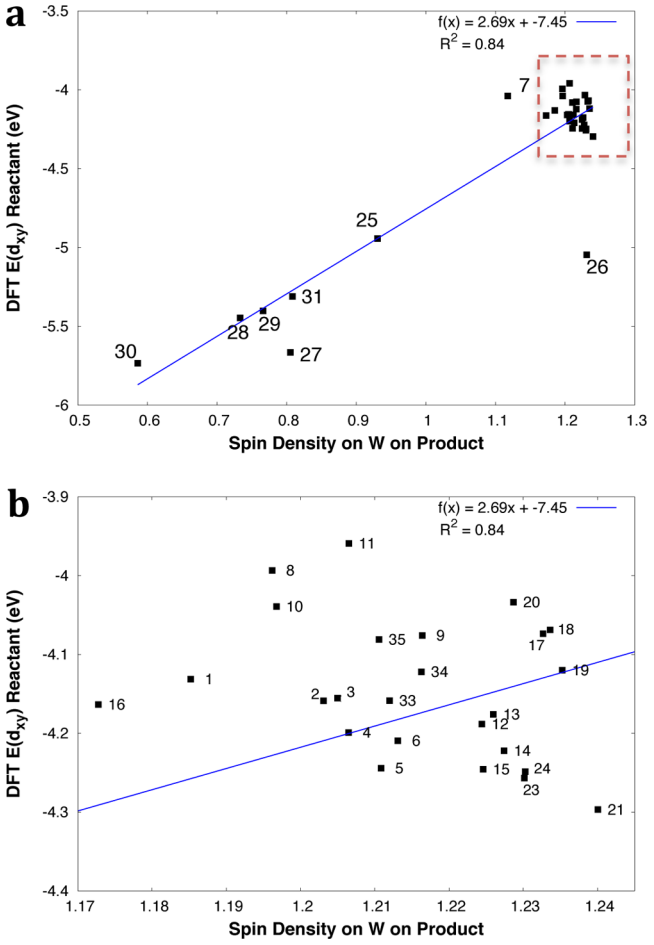

Figure 5. (a) Correlation between the energy of the d_{xy} frontier orbital and the spin density on W (omitting **22** and **32**) with an expansion (b) of the region with the red dashed-line box of the top figure. W spin densities of >1 reflect spin polarization of the alkylidyne group and antiferromagnetic coupling.

frontier orbitals of W(CPh)(dmpe)$_2$Cl (**12**) and W(CPh)-(CO)$_2$(tmeda)Cl (**28**), using data from the study presented here (Figure 4), shows that the orbital with d_{xy} character is more localized on W in **12** (−4.19 eV) than in **28** (−5.45 eV), where there is significant delocalization on the carbonyl ligands due to π-backbonding interactions. It is intuitively reasonable to expect, therefore, that the strong correlation between the oxidation potential and d_{xy} orbital energy would be paralleled by correlations between the d_{xy} orbital energy and measures of d_{xy}−L delocalization. However, it was found in the prior study that this correlation is not quantitative when calculated atomic orbital parentages of the d_{xy} redox orbital are used as the measure of delocalization.[9] For example, among the 27 W(CR)L$_4$X derivatives with phosphine or phosphite R groups (**1**−**21**, **23**, **24**, **26**, and **33**−**35**), the oxidation potential spans a range of 0.74 V (from −0.98 V for **8** to −0.24 V for **26**) and the calculated d_{xy} orbital energy varies by ∼1 V, yet the tungsten atomic parentage of the redox orbital ranges only from 72 to 77%. In the work presented here, we probed these relationships further by examining the spin density on the W center in the oxidized complexes (Table S11). As shown in Figure 5, there is a very coarse overall correlation between the energy of the d_{xy} frontier orbital and the spin density on W, with the CO-containing complexes (**25** and **27**−**31**) showing a reasonable linear correlation but the phosphine-containing W(CR)L$_4$X complexes (**1**−**21**, **23**, **24**, and **33**−**36**) appearing as a scatter plot. This result is very similar to that found for the correlation with the d_{xy} atomic parentage for the d^2 complexes. That these two calculated measures of delocalization (redox orbital tungsten parentage for the reduced compound and tungsten spin density for the oxidized compound) represent complementary probes of the redox orbital is reflected in the fact that they exhibit a reasonable linear correlation with each other (Figure S29). This plot would be predictive for complexes with very different spin densities [e.g., **12** vs **28** (Figure 4)] but could not differentiate very well between similar complexes [e.g., the W(CR)(phosphine)4X derivatives in Figure 5b].

In contrast to the ambiguous relationships of redox orbital parentage and spin density with redox orbital energy and oxidation potential, a relationship was observed between calculated oxidation potentials and W−X bond lengths for complexes with a given X ligand, for both reduced (d^2) reactants and oxidized (d^1) products. For the chloro derivatives of type W(CR)L$_4$Cl (**2**, **10**−**12**, **17**, **20**, **21**, **23**, **24**, **26**, and **34**−**36**) and W(CR)L$_n$(CO)$_{4-n}$Cl (**25**, **27**, **28**, and **32**), it is found that the longer the W−Cl bond, the more negative the

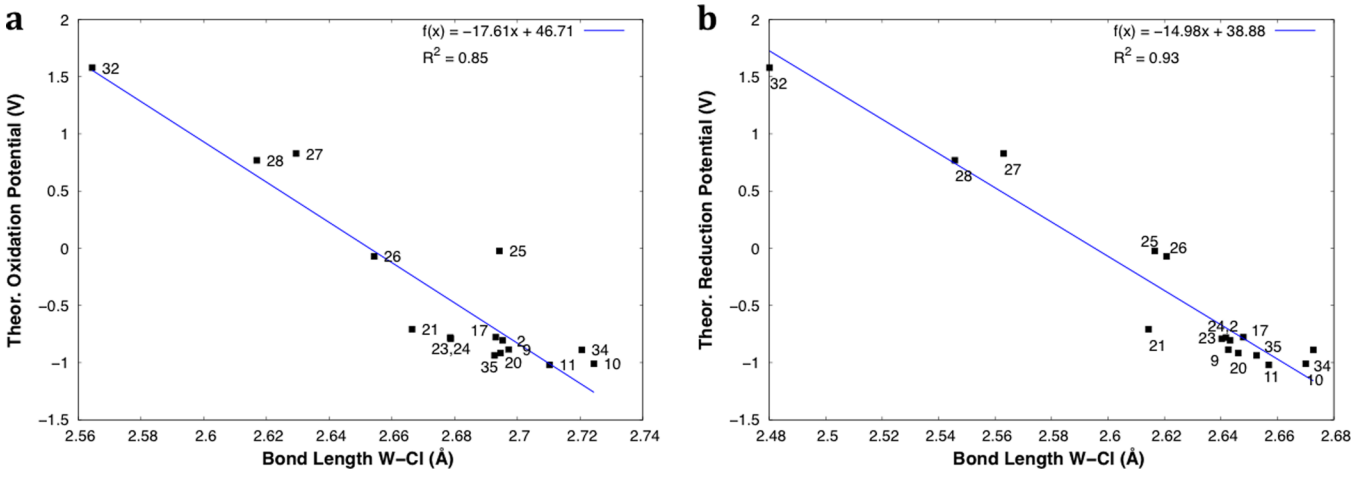

Figure 6. Correlation between oxidation potentials and W−Cl bond lengths for W−alkylidyne complexes, with Cl axial ligands, excluding **22**, for (a) reactants and (b) products.

DOI: 10.1021/acscatal.7b01636
ACS Catal. 2017, 7, 6134−6143

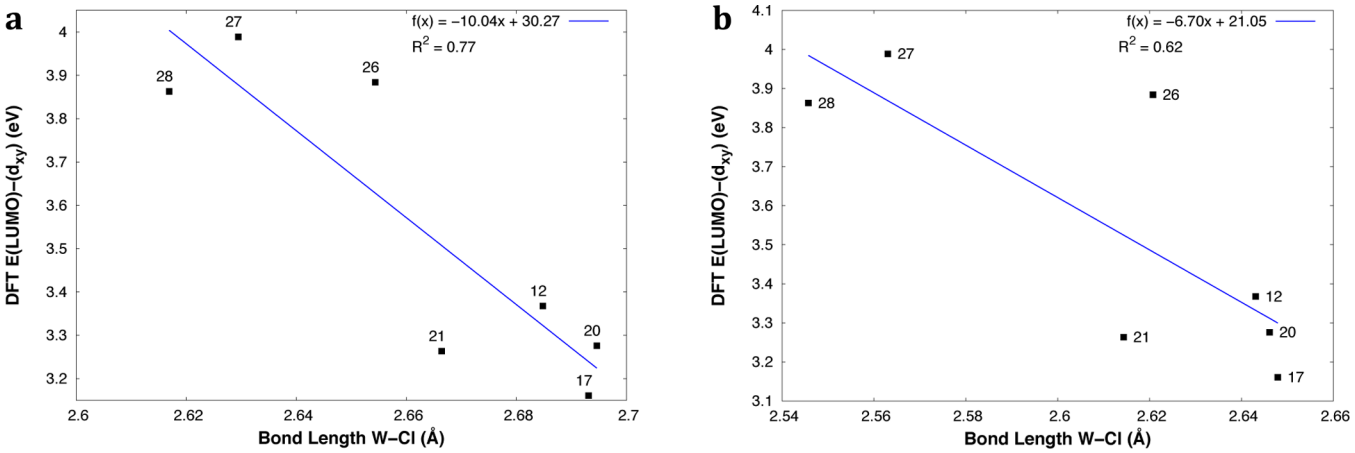

Figure 7. Correlation between the $E(\text{LUMO}) - E(d_{xy})$ gap and the W−Cl bond lengths for all complexes for which R = Ph for (a) reactants and (b) products.

Scheme 2. Illustration of the Stabilization through Backbonding of the Frontier Orbitals of Tungsten−Alkylidyne Complexes

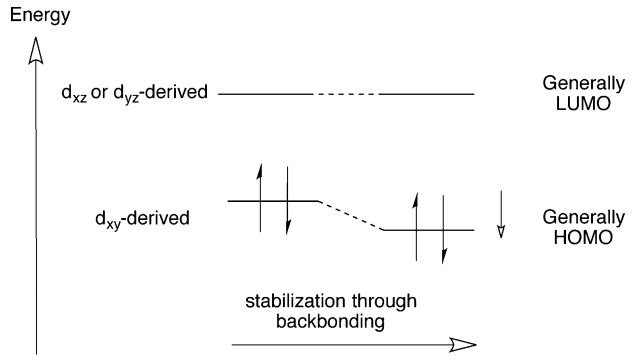

oxidation potential (Figure 6). The correlation is due to the effect of metal−ligand interactions on the relative energies of frontier orbitals and the resulting geometry change, analogous to the correlation between octahedral and square planar d orbital splittings. Equatorial ligands typically stabilize the HOMO with d_{xy} symmetry through π-backbonding interactions. The stabilization increases the energy gap between the HOMO and orbitals of d_{xz} and d_{yz} character (mainly the LUMO), which in turn reduces the W−X bond length. The change in bond length thus correlates with the increase in oxidation potential. This effect is related to the energy pattern of the frontier orbitals as opposed to either the steric and inductive *cis* influences found in cobaloximes and cobalamins[25−27] or the conservation of bond order[28−30] about the W. The axial W−X bond length is thus a descriptor of equatorial backbonding interactions that were found earlier to weakly report on the redox properties of the complex. The correlation appears to be weaker when the geometry is relaxed in the dielectric continuum model (Figure S31), though an expanded data set would be needed to confirm this point.

Figure 7 shows the correlation between the $E(\text{LUMO}) - E(d_{xy})$ gap and the calculated W−Cl bond length for all complexes for which R = Ph. The observed correlations confirm that the W−X bond length reports on the energy gap between frontier orbitals that determine the oxidation potential of the complexes, as illustrated in Scheme 2. A similar correlation is found for complexes for which X = Br, as shown in Figure S30. Therefore, the W−X bond length could be used as a structural marker for designing complexes with specific oxidation potentials. The effect in the oxidized products is even more evident as the W−Cl bond length differences are slightly larger.

We note that the W−X bond length is unique with regard to correlations with the redox properties of these complexes. Other bond lengths in the complexes do not show significant correlation with the oxidation potential of the complex. For example, the W−P bond lengths for complexes with phosphine ligands vary within only a narrow range from 2.47 Å (**8**) to 2.53 Å (**27**) and the W≡C(R) bond lengths for all complexes vary within only a narrow range from 1.79 Å (**5**) to 1.83 Å (**33**). As has been noted elsewhere, W−X bond lengths of tungsten−alkylidyne complexes tend to be unusually long compared to those of non-alkylidyne−tungsten compounds because of the strong *trans* influence of the alkylidyne ligand.[31,32] This may also make them especially sensitive to subtle electronic−structural effects that are important to physical properties such as redox potentials.

CONCLUSIONS

We have demonstrated the ability of a combined electrochemical and computational analysis of tungsten−alkylidyne complexes to provide a basis for understanding their redox properties on the basis of the symmetries of metal−ligand interactions and the relative contributions of ionization and solvation energies. Good agreement between theory and experiment can be achieved with comparatively standard levels of theory [B3LYP/(LANL2DZ,6-311G*)], suggesting that these approaches can be readily applied to the design of new complexes with specific redox potentials. It is striking that the strong linear correlation between the oxidation potential and energy of the redox orbital is not mirrored by broad correlations with measures of redox orbital delocalization, such as the local spin density of the oxidized product. However, the orbital−energy correlation is manifest in the W−X bond length, which serves as a structural descriptor for the redox properties of the complex. The observed correlations should be particularly valuable for the design of new tungsten−alkylidyne complexes with specific redox properties, which is of interest for their applications as photoreductants[33] and for the activation of H_2.[11]

DOI: 10.1021/acscatal.7b01636
ACS Catal. 2017, 7, 6134−6143

■ ASSOCIATED CONTENT

Supporting Information

The Supporting Information is available free of charge on the ACS Publications website at DOI: 10.1021/acscatal.7b01636.

Synthesis and characterization (^{13}C, ^{31}P, ^{1}H, and ^{19}F NMR, mass spectrometry, and elemental analysis) of **33**, **35**, and their precursor complexes, single-crystal X-ray diffraction studies of **12**, **33**, and **35**, electrochemistry (CV and DPV), oxidation potentials for all complexes studied along with partitioned contributions, comparison and discussion of the theoretical and experimental geometric parameters for **12**, **21**, **21**$^{+}$, **33**, and **35**, computed free energies and redox potentials, analysis of the error between theory and experiment, comparison of $E(d_{xy})$ values to those in previous work with these complexes, calculated HOMO reactant energies, calculated spin densities and their symmetries, correlation between gas-phase ionization potentials and experimental oxidation potentials in solution, differences in solvation energy between the reactant and product, overall comparison of orbital energies with potentials, correlation between atomic parentage and oxidized W spin density, correlation between the $E(\mathrm{LUMO}) - E(d_{xy})$ gap and W−Br bond lengths, analysis of results obtained upon optimization in solution, and additional references (PDF)

Theoretical coordinates in the form of .xyz files labeled with the electronic energy in Hartrees (PDF)

Details of the X-ray crystal structure for **12** (CIF)

Details of the X-ray crystal structure for **33** (CIF)

Details of the X-ray crystal structure for **35** (CIF)

■ AUTHOR INFORMATION

Corresponding Authors

*E-mail: victor.batista@yale.edu. Phone: (203) 432-3925. Fax: (203) 432-6144.

*E-mail: mhopkins@uchicago.edu. Phone: (773) 702-6490.

ORCID

Benjamin Rudshteyn: 0000-0002-9511-6780

Hunter B. Vibbert: 0000-0001-9591-7150

Michael D. Hopkins: 0000-0002-0697-8152

Victor S. Batista: 0000-0002-3262-1237

Notes

The authors declare no competing financial interest.

■ ACKNOWLEDGMENTS

V.S.B. acknowledges support from AFOSR Grant FA9550-13-1-0020 and supercomputing time from NERSC and from the high-performance computing facilities at Yale University. M.D.H. acknowledges financial support from the U.S. Department of Energy, Office of Basic Energy Sciences, Solar Photochemistry Program (Grant DE-FG02-07-ER15910). B.R. acknowledges support from a National Science Foundation Graduate Research Fellowship under Grant DGE-1122492. We thank Prof. Robert H. Crabtree, Dr. Junming Ho, and Dr. Andreas Markmann for helpful comments and Dr. Alexander Filatov for determining the crystal structures.

■ REFERENCES

(1) Konezny, S. J.; Doherty, M. D.; Luca, O. R.; Crabtree, R. H.; Soloveichik, G. L.; Batista, V. S. *J. Phys. Chem. C* **2012**, *116*, 6349−6356.

(2) Ho, J. *Phys. Chem. Chem. Phys.* **2015**, *17*, 2859−2868.

(3) Ashford, D. L.; Gish, M. K.; Vannucci, A. K.; Brennaman, M. K.; Templeton, J. L.; Papanikolas, J. M.; Meyer, T. J. *Chem. Rev.* **2015**, *115*, 13006−13049.

(4) Sattler, W.; Henling, L. M.; Winkler, J. R.; Gray, H. B. *J. Am. Chem. Soc.* **2015**, *137*, 1198−1205.

(5) Arias-Rotondo, D. M.; McCusker, J. K. *Chem. Soc. Rev.* **2016**, *45*, 5803−5820.

(6) Shaw, M. H.; Twilton, J. T.; MacMillan, D. W. C. *J. Org. Chem.* **2016**, *81*, 6898−6926.

(7) O'Hanlon, D. C.; Cohen, B. W.; Moravec, D. B.; Dallinger, R. F.; Hopkins, M. D. *J. Am. Chem. Soc.* **2014**, *136*, 3127−3136.

(8) Da Re, R. E.; Hopkins, M. D. *Coord. Chem. Rev.* **2005**, *249*, 1396−1409.

(9) Haines, D. E.; O'Hanlon, D. C.; Manna, J.; Jones, M. K.; Shaner, S. E.; Sun, J.; Hopkins, M. D. *Inorg. Chem.* **2013**, *52*, 9650−9658.

(10) Lovaasen, B. M.; Lockard, J. V.; Cohen, B. W.; Yang, S.; Zhang, X.; Simpson, C. K.; Chen, L. X.; Hopkins, M. D. *Inorg. Chem.* **2012**, *51*, 5660−5670.

(11) Morales-Verdejo, C. A.; Newsom, M. I.; Cohen, B. W.; Vibbert, H. B.; Hopkins, M. D. *Chem. Commun.* **2013**, *49*, 10566−10568.

(12) Furno, F.; Fox, T.; Schmalle, H. W.; Berke, H. *Organometallics* **2000**, *19*, 3620−3630.

(13) Lee, C.; Yang, W.; Parr, R. G. *Phys. Rev. B: Condens. Matter Mater. Phys.* **1988**, *37*, 785−789.

(14) Frisch, M. J.; Trucks, G. W.; Schlegel, H. B.; Scuseria, G. E.; Robb, M. A.; Cheeseman, J. R.; Scalmani, G.; Barone, V.; Mennucci, B.; Petersson, G. A.; Nakatsuji, H.; Caricato, M.; Li, X.; Hratchian, H. P.; Izmaylov, A. F.; Bloino, J.; Zheng, G.; Sonnenberg, J. L.; Hada, M.; Ehara, M.; Toyota, K.; Fukuda, R.; Hasegawa, J.; Ishida, M.; Nakajima, T.; Honda, Y.; Kitao, O.; Nakai, H.; Vreven, T.; Montgomery, J. A., Jr.; Peralta, J. E.; Ogliaro, F.; Bearpark, M.; Heyd, J. J.; Brothers, E.; Kudin, K. N.; Staroverov, V. N.; Kobayashi, R.; Normand, J.; Raghavachari, K.; Rendell, A.; Burant, J. C.; Iyengar, S. S.; Tomasi, J.; Cossi, M.; Rega, N.; Millam, N. J.; Klene, M.; Knox, J. E.; Cross, J. B.; Bakken, V.; Adamo, C.; Jaramillo, J.; Gomperts, R.; Stratmann, R. E.; Yazyev, O.; Austin, A. J.; Cammi, R.; Pomelli, C.; Ochterski, J. W.; Martin, R. L.; Morokuma, K.; Zakrzewski, V. G.; Voth, G. A.; Salvador, P.; Dannenberg, J. J.; Dapprich, S.; Daniels, A. D.; Farkas, Ö.; Foresman, J. B.; Ortiz, J. V.; Cioslowski, J.; Fox, D. J. *Gaussian 09*; Gaussian, Inc.: Wallingford, CT, 2009.

(15) Hay, P. J.; Wadt, W. R. *J. Chem. Phys.* **1985**, *82*, 299−310.

(16) Marenich, A. V.; Cramer, C. J.; Truhlar, D. G. *J. Phys. Chem. B* **2009**, *113*, 6378−6396.

(17) Cramer, C. J. *Essentials of Computational Chemistry: Theories and Models*, 2nd ed.; John Wiley & Sons: West Sussex, U.K., 2004; p 355.

(18) Ribeiro, R. F.; Marenich, A. V.; Cramer, C. J.; Truhlar, D. G. *J. Phys. Chem. B* **2011**, *115*, 14556−14562.

(19) Ho, J.; Klamt, A.; Coote, M. L. *J. Phys. Chem. A* **2010**, *114*, 13442−13444.

(20) Ho, J.; Ertem, M. Z. *J. Phys. Chem. B* **2016**, *120*, 1319−1329.

(21) Bard, A. J.; Faulkner, L. R. *Electrochemical Methods: Fundamentals and Applications*; John Wiley & Sons: New York, 2001, p 261.

(22) Zhang, L.; Gamasa, M. P.; Gimeno, J.; Guedes da Silva, M. F. C.; Pombeiro, A. J. L.; Graiff, C.; Lanfranchi, M.; Tiripicchio, A. *Eur. J. Inorg. Chem.* **2000**, *2000*, 1707−1715.

(23) Grimme, S.; Ehrlich, S.; Goerigk, L. *J. Comput. Chem.* **2011**, *32*, 1456−1465.

(24) In the following discussion, the cationic compound $[W(CPh)(dppe)_2(NCMe)]^+$ (**22**) is excluded, because of the difference in charge relative to the otherwise neutral compounds in this study.

(25) De March, M.; Demitri, N.; Geremia, S.; Hickey, N.; Randaccio, L. *J. Inorg. Biochem.* **2012**, *116*, 215−227.

DOI: 10.1021/acscatal.7b01636
ACS Catal. 2017, 7, 6134−6143

(26) Govender, P. P.; Navizet, I.; Perry, C. B.; Marques, H. M. *Chem. Phys. Lett.* **2012**, *550*, 150−155.
(27) Navizet, I.; Perry, C. B.; Govender, P. P.; Marques, H. M. *J. Phys. Chem. B* **2012**, *116*, 8836−8845.
(28) Johnston, H. S.; Parr, C. *J. Am. Chem. Soc.* **1963**, *85*, 2544−2551.
(29) Santen, R. A. *Theoretical Heterogeneous Catalysis*; World Scientific Publishing: Teaneck, NJ, 1991; p 205.
(30) Brown, I. D. *J. Phys. Chem. A* **2011**, *115*, 12638−12645.
(31) Jacobsen, H.; Berke, H. *J. Chem. Soc., Dalton Trans.* **2002**, 3117−3122.
(32) Vaughan, W. M.; Abboud, K. A.; Boncella, J. M. *Organometallics* **1995**, *14*, 1567−1577.
(33) Moravec, D. B.; Hopkins, M. D. *Chem. - Eur. J.* **2013**, *19*, 17082−17091.

DOI: 10.1021/acscatal.7b01636
ACS Catal. 2017, 7, 6134−6143